Dynamic Contrast Enhanced MRI Detection of a Central Defect in Clear Cell Renal Cell Carcinoma Correlates with a Tumor Scar and Lower Tumor Proliferation Rate

Yue Zhang[1], Payal Kapur[2,3], Qing Yuan[1], Ananth Madhuranthakam[1,4], Ingrid Carvo[5], Sabina Signoretti[5], Ivan Dimitrov[6], Yin Xi[1], Katherine Wicks[1], Jeffrey Cadeddu[1,3], Vitaly Margulis[3], James Brugarolas[7,8], and Ivan Pedrosa[1,4]

[1]Radiology, University of Texas Southwestern Medical Center, Dallas, Texas, United States, [2]Pathology, University of Texas Southwestern Medical Center, Dallas, Texas, United States, [3]Urology, University of Texas Southwestern Medical Center, Dallas, Texas, United States, [4]Advanced Imaging Research Center, University of Texas Southwestern Medical Center, Dallas, Texas, United States, [5]Pathology, Brigham and Women's Hospital, Boston, Massachusetts, United States, [6]Philips Medical Systems, Cleveland, Ohio, United States, [7]Internal Medicine, University of Texas Southwestern Medical Center, Dallas, Texas, United States, [8]Developmental Biology, University of Texas Southwestern Medical Center, Dallas, Texas, United States

INTRODUCTION: Coagulative tumor necrosis at histopathology is associated with worse prognosis in clear cell tumors, the most common subtype of renal cell carcinoma (RCC)[1]. Macroscopic tumor necrosis on MRI is frequently described as a central, stellate-shaped, non-enhancing area with high signal intensity on T2-WI and this finding also correlates with worse prognosis in clear cell RCC[2]. We have recently observed, however, a correlation between this imaging finding and a central scar at histopathology in clear cell RCC. Our aim was to correlate the presence of MRI-suspected tumor necrosis with morphologic findings in clear cell RCC and to propose a potential pathophysiologic mechanism for the presence of this imaging feature.

MATERIALS AND METHODS

Patients and MRI Protocol: This was a prospective, IRB-approved, HIPAA-compliant study. Fifty patients with known solid renal masses signed informed consent prior to imaging. Of these, 34 patients had a clear cell RCC confirmed after nephrectomy and represent our study population. Patients underwent 3T dual-transmit MRI with a 16-channel SENSE-XL-Torso coil (Achieva, Philips Medical System). Axial and coronal T2-weighted half-Fourier single-shot turbo spin-echo images (T2WI) were acquired followed by dynamic contrast enhanced (DCE) MRI with a coronal 3D spoiled gradient echo acquisition (SPGR)[TR/TE = 3/1.53 ms, FA = 10°, number of average = 1, slice thickness = 5mm, FOV = 408×408 mm2, matrix = 288×288, bandwidth = 1326 Hz/pixel]; and temporal resolution of 5 sec. To minimize respiratory motion, three consecutive dynamic phases were obtained within each 15-sec breath-held acquisition period. A 15-sec period of free-breathing was allowed between consecutive acquisition periods. Three baseline SPGR acquisitions were followed by a bolus of 0.1 mmol/kg of gadobutrol (Gadavist; Bayer Healthcare Pharmaceuticals) using a power injector at a rate of 2 cc/sec followed by a 20 cc saline flush at 2 cc/sec. The same SPGR sequence was used to generate a T1 map ($T1_0$) prior to contrast injection with three separate acquisitions (flip angles 10°, 5°, and 2°). *Image Analysis:* All images were analyzed with an open-source DICOM viewer (Osirix X, version 5.6, 64bit, Bernex, Switzerland). Maximum tumor size was measured based on 3 orthogonal measurements on T2WI. DCE images were processed with a motion correction algorithm using commercial software VersaVue Enterprise (iCAD, Inc., Nashua, NH), to generate motion corrected DCE-derived vascular maps: K^{trans}, K_{ep}, Ve, Vp, $iAUC_{90sec}$ and $T1_0$. Using a slice location through the center of the mass, a radiologist with 14 years' experience in body MRI divided all cases into two groups: tumor without (NoScar) and with a scar (Scar). Scar tumors demonstrated a stellate, non-enhancing central defect on the later phase (300sec post-injection) of the DCE images. Masses in the NoScar group exhibited diffuse enhancement without visible defect. *Histopathology:* All patients underwent partial (n=23) or radial (n=11) nephrectomy after MRI (mean MRI-surgery interval 6.0±3.7day). Renal masses were anatomically oriented after surgery with the use of fiducial markers placed during surgery and then bivalded through the center to match the location of the MRI slice. Tumor slides were obtained from the selected anatomic location and stained with hematoxylin-eosin for assessment of nuclear (Fuhrman) tumor grade. Additional tumor slides were stained with Ki-67 to assess tumor cell proliferation. The percentage of nuclei that stained with Ki-67 was measured using a pattern-recognition software package (Aperio Spectra plus and Scanscope). *Statistics:* The percentage of positive nuclei was normalized to tumor size. Non-paired t-test was performed for normalized percentage nuclei and for tumor Fuhrman grade between the two groups. The Spearman rank-order correlation was used to assess the correlation between scar size and tumor size. (P<0.05 considered statistically significant).

RESULTS: There were 23 masses in the Scar group and 11 masses in the NoScar group. Fuhrman grade between the two groups was not significantly different (P=0.5310). Tumors in the scar group (6.7±2.5 cm) were larger than tumors in the NoScar (3.9±1.2 cm) group (P=0.0005). K^{trans}(P=0.3316), K_{ep}(P=0.4929), Ve(P=0.3039), Vp(P=0.3316), $iAUC_{90sec}$(P=0.6060) and $T1_0$(P=0.5671) between the two groups were not significantly different. The central non-enhancing defect corresponded to a central scar in all tumors in the Scar group. Nine of 23 tumors in Scar group, and 2 of 11 tumors in NoScar group had coagulative necrosis histologically (P=0.2263). Ki-67 staining was available in 19 RCCs in Scar group and 10 RCCs in NoScar group. The central defect in the Scar group correlated macroscopically with tan-white, glistening, firm stellate area and consisted of fibrotic and edematous hypo cellular stroma microscopically. **Fig.1** shows representative images of a Scar tumor. The tumor size-normalized percentage positive nuclei on Ki-67 stains in Scar group was significantly lower than that of NoScar group (P=0.0006) (**Fig.2**). The area of the scar was significantly correlated (P=0.0001) with tumor size (**Fig.3A**). For all clear cell RCCs, the tumor size-normalized percentage positive nuclei negatively correlated with tumor size (**Fig.3B**).

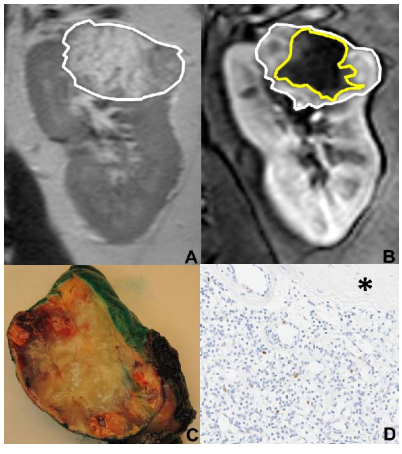

Fig.1: A clear cell RCC with scar. (**A**) T2W. (**B**) DCE image shows scar area (yellow circle). (**C**) Gross examination shows a white and firm scar, different than central necrosis. (**D**) Ki-67 staining shows very few positive nuclei in viable portion of the tumor, adjacent to the scar (*).

Fig. 3

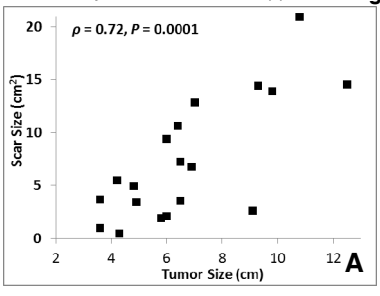

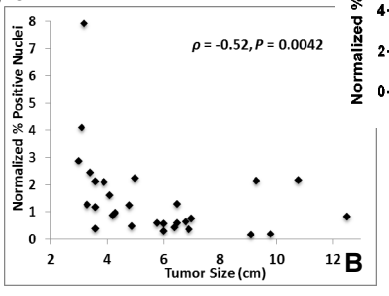

Fig. 2

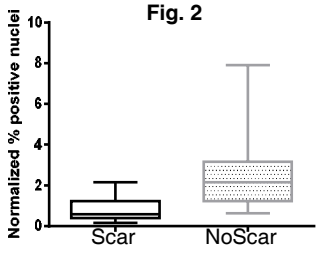

REFERENCES: 1. Delahunt et al. Am J Surg Pathol. 2013;
2. Beddy et al. Clin Genitourin Cancer. 2014

ACKNOWLEDGEMENT: This study was supported by the grant NIH/NCI 1R01CA154475-04.

CONCLUSION: Our study confirmed that central non-enhancing defects in clear cell RCC on MRI represent a tumor scar instead of macroscopic necrosis. Tumors with scars are larger and demonstrate statistically significant lower proliferation rates than those without scars. We hypothesize that this scar is the result of rapid enlargement of the tumor and overgrowth of its vascular supply leading to a central infarct and formation of a scar during a subsequent reparative phase.